Arch. Metall. Mater. **63** (2018), 1, 181-189

DOI: 10.24425/118926

Ł. RAKOCZY**#, M. GRUDZIEŃ*, A. ZIELIŃSKA-LIPIEC**

CONTRIBUTION OF MICROSTRUCTURAL CONSTITUENTS ON HOT CRACKING OF MAR-M247 NICKEL BASED SUPERALLOY

The aim of this study is to investigate influence of selected parameters of gas tungsten arc welding on microstructure of MAR-M247 nickel based superalloy originating from turbine vane. MAR-M247 is a precipitation-strengthened superalloy which is widely used in aerospace engines. The main strengthening phase in this material is ordered $L1_2$ intermetallic γ' phase Ni_3(Al, Ti). The surface of alloy was modified by electric arc in order to present microstructural changes in weld and heat affected zone. Investigation of the heat affected zone revealed that constitutional liquation of γ' particles and primary carbides is responsible for the formation of a liquid grain boundary layer which finally contributed to cracking. Scanning electron microscopy indicated high susceptibility to cracking of MAR-M247 alloy which is connected with high content of γ'-formers aluminum and titanium.

Keywords: superalloys, liquation cracking, gamma prime, MAR-M247

1. Introduction

MAR-M247 belongs to nickel based superalloys widely used in aeroengines for components such as airfoil, blades in high pressure turbine (HPT) and vanes in low pressure turbine (LPT). Superalloys in service conditions must withstand considerable stress and harsh corrosion environment. Metallurgical development of aircraft engines is coupled with the first high temperature Ni-alloys design [1-3]. In order to ensure microstructure stability and sufficiently high mechanical properties, alloys are provided with complex alloying system containing γ'-formers, aluminum and titanium. Additional increasing of mechanical properties originates from carbides precipitated mainly along grain boundaries and solid solution strengthening [4]. Intermetallic phase denoted as γ' have a very good crystallographic matching with γ-matrix which leads to a low surface energy and so cause very low coarsening rate of precipitates. Lattice parameter of matrix and γ' particles depends on the quantity and type of elements in superalloy. Alloying elements can be divided into these phase in which various partition and change lattice parameter of γ and γ' in different way [5-7]. Gas tungsten arc welding (GTAW) and advanced techniques such as laser beam welding are widely used to manufacturing and repair gas turbine components made of both ferrous and non-ferrous alloys. Welding is desirable economical and versatile technique because defects may be scrapped and repaired. However, welding of cast nickel based superalloys has been a difficult and complex issue due to relatively high susceptibility to cracking in fusion zone (FZ) and heat affected zone (HAZ) [8-10]. Liquation and cracking along grain boundaries in HAZ is observed in many alloy systems including nickel alloys, maraging steels and aluminum alloys. Liquating phases in such groups of materials are various; γ'-phase [11], carbides and nitrocarbides [12], sulfides [13]. Low ductility of base metal due to solute rich film at grain boundaries and stress originating from welding thermal cycle can result formation of microfissuring. Creation of liquid along grain boundaries has been attributed to the constitutional liquation of second phase particles. Mechanism of this phenomenon was firstly proposed by Pepe and Savage [14] based on investigation carried out on 18Ni maraging steel. Interface melting occurs by constitutional liquation below solidus temperature and is detrimental to cracking resistance because extends solidus-liquidus temperature range. Very little information is available on open literature about constitutional liquation phenomena and hot cracking including solidification in fusion zone and liquation cracking in HAZ in MAR-M247 alloy. This investigation has been carried out in order to clarify the influence of welding process on microstructure and cracking morphology.

2. Experimental procedure

The material for the experiment was taken from the investment casted turbine vane (location is shown in Figure 1). The chemical composition of base metal determined using optical

* FOUNDRY RESEARCH INSTITUTE, 73 ZAKOPIAŃSKA STR., 30-418 CRACOW, POLAND
** AGH UNIVERSITY OF SCIENCE AND TECHNOLOGY, FACULTY OF METALS ENGINEERING AND INDUSTRIAL COMPUTER SCIENCE, DEPARTMENT OF PHYSICAL AND POWDER METALLURGY, AL. MICKIEWICZA 30, 30-059 KRAKÓW, POLAND
# Corresponding author: lrakoczy@agh.edu.pl

emission spectroscopy analyzer is presented in Table 1. The alloy was subjected to surface modification using gas tungsten arc welding method. The process was performed with the use of Oerlikon welding machine (parameters are summarized in Table 2).

Fig. 1. Location of base metal originating from gas turbine vane

TABLE 1

Chemical composition of MAR-M247

Element [% wt.]	W	Co	Cr	Al	Ta	Hf	Ti	Mo	C	Ni
MAR--M247	10.19	9.92	8.40	5.58	3.12	1.11	0.92	0.64	0.13	Bal.

TABLE 2

Selected welding parameters

Current [A]	Voltage [V]	Travel speed [mm/min]	Efficiency k [15]	Heat input [kJ/mm]	Electrode	Shielding gas
55	12	250	0.6	0.09	2%Th	Argon

Sample was grinded using sandpaper and polished on diamond suspension to avoid differences in roughness of weld pool area. Macrostructure of base metal was revealed by chemically etched with Marble's reagent. Surface for microstructure investigation was etched electrolytically in 10% $Cr0_3$ reagent. Observations were conducted on surface parallel to welding direction. The microstructural characterization of the sample was performed using light microscopy (LM), scanning electron microscopy (SEM) equipped with EDS detector, hardness survey and X-ray phase analysis.

3. Results and discussion

3.1. Base metal characterization

As shown in Figure 2a on unetched sample, MAR-M247 superalloy contains carbides characterized by different shape from blocky to carbides in an arrangement termed Chinese script. Carbides like Chinese script (Fig. 2b) precipitated in the final stage of solidification via eutectic reaction with γ-matrix inside the alloy. These carbides are composed of three separated parts. The central cores with elongated arms are formed but script arms end in enlarged angular heads. The magnitude of these structures and proportion of head to core and arm have been found to be connected with solidification conditions.

Macroetching of base metal revealed that turbine vane has been delivered in polycrystalline form (Fig. 3). Porosity and worst internal segregation including nonmetallic inclusions were not detected. It has been found that the casting is made correctly and can be used as a material for further investigation.

The etched microstructure of cast superalloy consists of precipitation of γ' intermetallic phase within dendrite core and in the interdendritic spaces (Fig. 4a). Along interdendritic region carbides (Fig. 4b) and eutectic islands γ/γ' are present. Creation of islands occurs due to complex chemical composition and the resulting microsegregation during solidification of superalloy. Volume fraction of eutectic islands is substantially higher in comparison with other nickel based superalloys [16].

Microstructure is characterized by relatively large inhomogenity. Dendrite cores consist of cubic γ' divided by γ-matrix channels (Fig. 5a). Inside eutectic islands γ' take a different shape from cubic to large irregular polygons (Fig. 5b). In interdendritic regions γ' particles (γ/γ' eutectic islands) are formed directly from residual melt. Microstructure investigation revealed presence of significant amount of γ'. Investigation carried out by

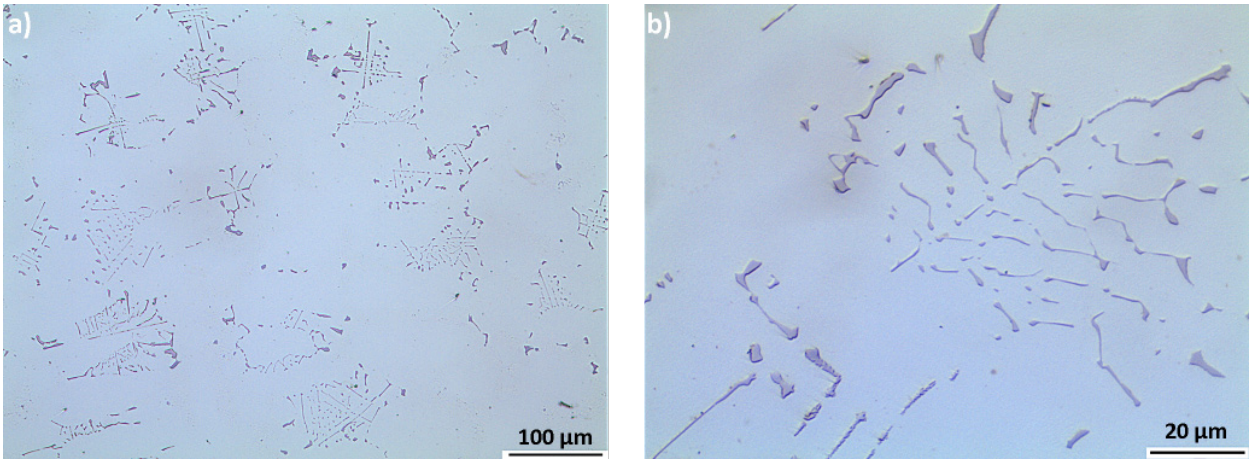

Fig. 2. Morphology of primary carbides in MAR-M247 superalloy: a) general distribution; b) Chinese script morphology. LM

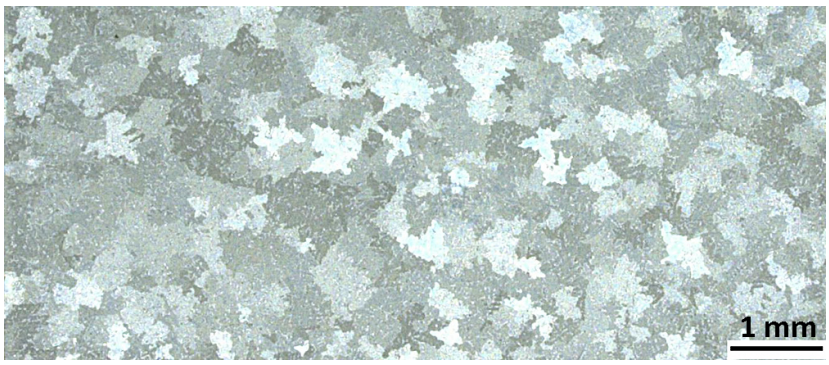

Fig. 3. Macrostructure of etched sample. LM

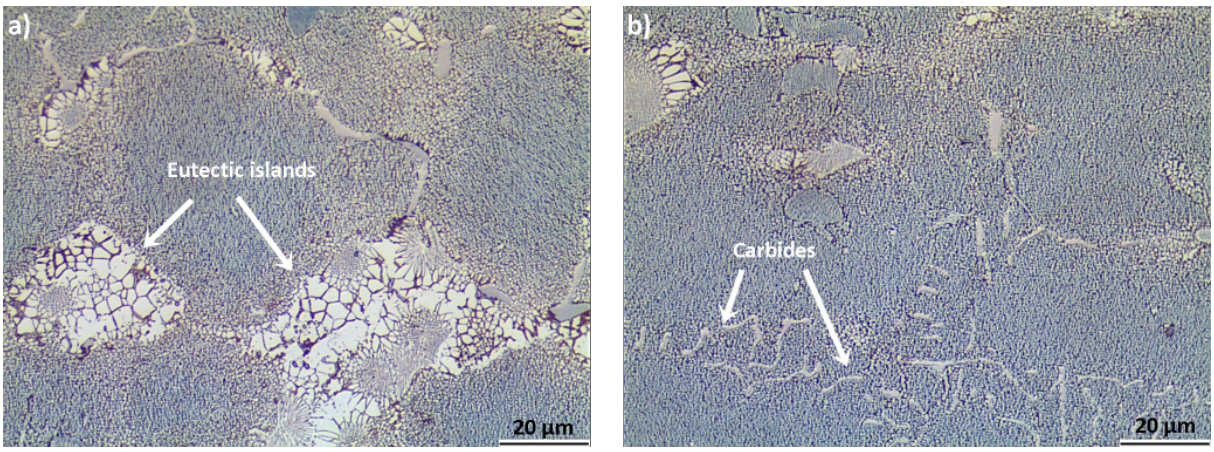

Fig. 4. Microstructure of alloy: a) eutectic islands γ/γ'; b) carbides. LM

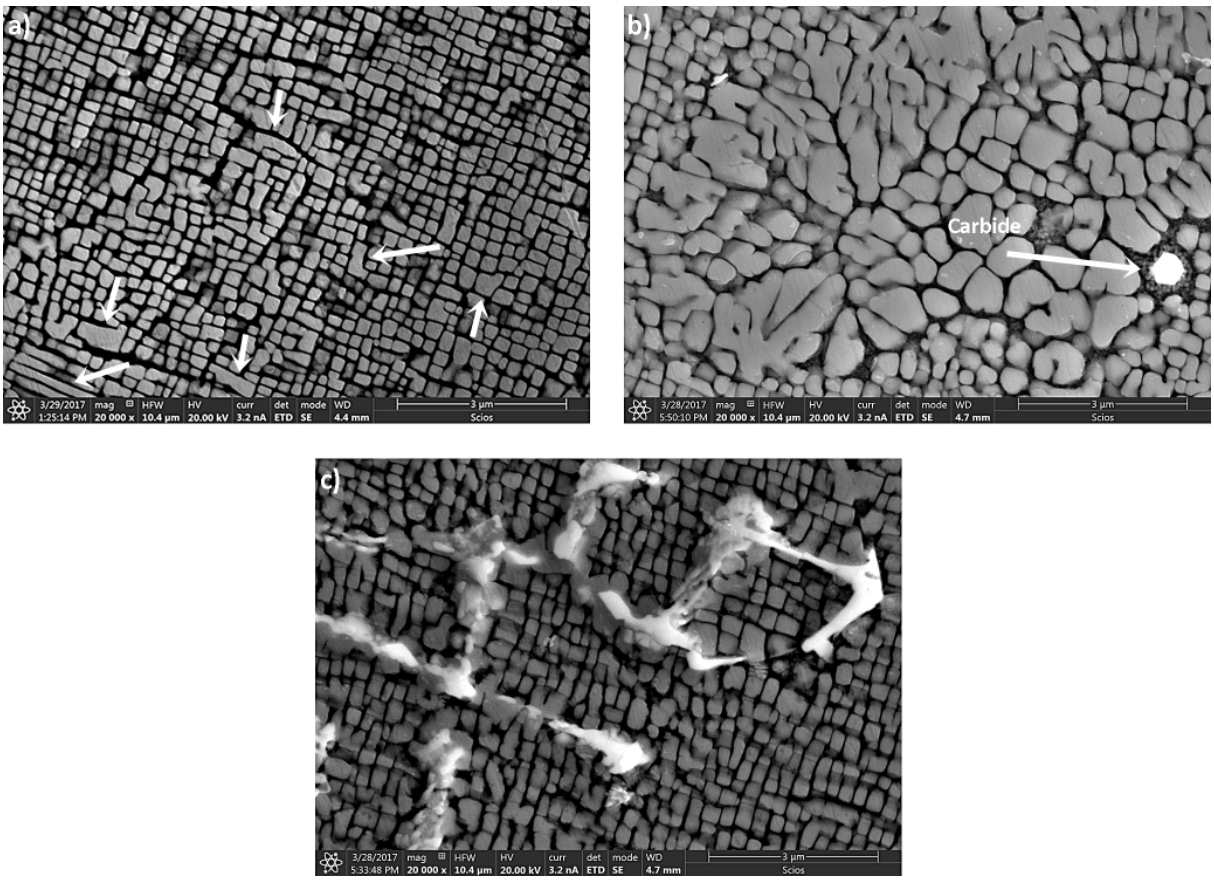

Fig. 5. Microstructure constituents in alloy: a) γ' particles; b) eutectic γ/γ'; c) carbides. SEM

Baldan shows that volume fraction of main strengthening phase is approximately 60% [17]. The hardness value obtained during survey is 465HV5. The difference in phase contrast of carbides (blocky and Chinese script morphology) indicates differing in chemical composition. Blocky carbides located inside eutectic islands are surrounded by very fine gamma prime particles, while more complex shape carbides are surrounded by thick precipitations (Fig. 5c).

By X-ray diffraction (Fig. 6) γ, γ' and MC-type carbides enriched in Ta and Hf were identified. Separating of γ, γ' (100) and γ, γ' (200) peaks is connected with differences in lattice parameter of γ and γ'. The lattice misfit of the phases (constraint misfit δ) was calculated as [18]:

$$\delta = \frac{2\left(a_{\gamma'} - a_{\gamma}\right)}{a_{\gamma'} + a_{\gamma}} \qquad \text{(Eq. 1)}$$

Lattice misfit corresponds with shape of γ' particles and based on literature [19] data is usually less than 1% for superalloys. For cubic particles misfit coefficient is equal 0.5-1%, in turn for spherical is 0-0.5%. Above 1% intermetallic phase γ' has a plate-like shape. Microstructural analysis revealed large amount of particles with different shape than cubic which explain separating of peaks on XRD spectrum.

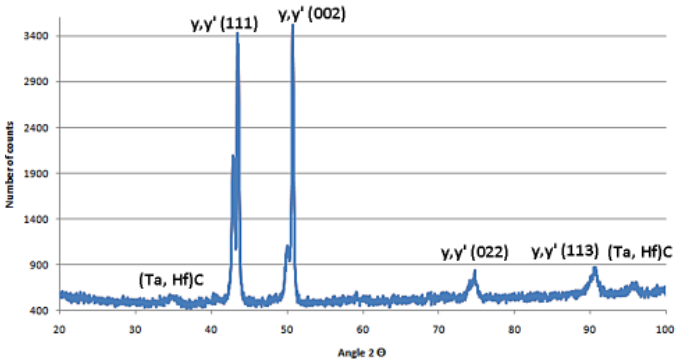

Fig. 6. X-ray spectrum of MAR-M247. Radiation Cu K_{α}

3.2. Microstructural changes after surface modification

Microstructural changes of MAR-M247 superalloy after GTAW surface modification are shown in Figure 7. Three characteristic regions are marked, ie base material, heat affected zone and fusion zone. They were subjected to further investigation with the use scanning electron microscope and results are presented in Figs. 8-10. No significant microstructural changes are observed in heat affected zone at 600 μm from fusion line. Precipitates γ' in dendrite cores, eutectic islands and around carbides were probably locally dissolved (Fig. 8a-c). Substantial microstructural changes are observed in the heat affected zone near the fusion line (Fig. 9). The temperature during the welding process was much higher there. This is visible in the form of the change in the geometry and size of the γ' precipitates (Fig. 9a-b). The heat contributed to their strong dissolution, and so the temperature exceed γ' solvus. During cooling from the supersaturated solution, re-precipitation of γ' has began (Fig. 9c). As a result of the alloying elements segregation, the melting temperature of the eutectic is lower than that of the surrounding material. In the investigated area incipient melting was not observed. Differential thermal analysis conducted by Baldan revealed that γ' solvus is 1225°C, while incipient melting temperature is 1319°C [17]. In the fusion zone very fine γ' phase is surrounded by γ. At the grain boundaries Chinese script carbides created via eutectic reaction with the γ matrix are observed (Fig. 10a-b). Large irregular γ' particles are observed only inside eutectic islands (Fig. 10c). According to the work of Baldan [17] the liquidus temperature of the MAR-M247 is 1343°C, which is a value close to the thermodynamic calculations according to which it is equal to 1360°C.

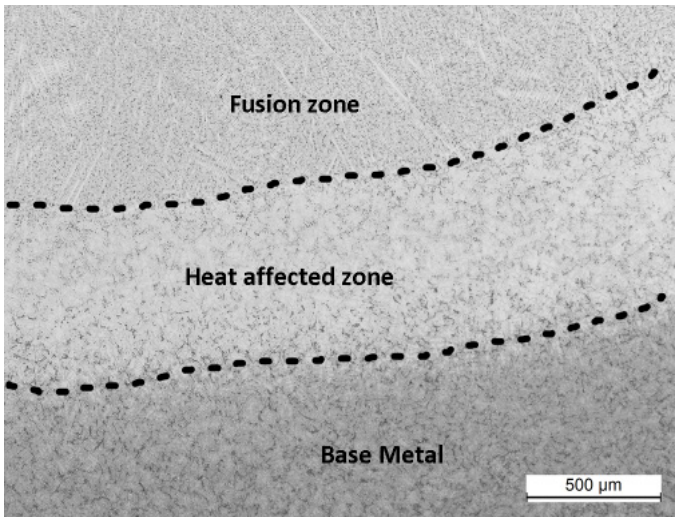

Fig. 7. Microstructure of specimen after surface modification. LM

3.3. Morphology and cracking characteristics

In the sample many hot cracks were observed including one that initiated in fusion zone and propagated via fusion line to heat affected zone (Fig. 11). Formation of liquation cracking in HAZ near the fusion line was assisted by a crack formed earlier during solidification of the melting area, as evidenced by its relatively large width.

General view of hot crack in fusion zone is shown in Fig. 12a. Along crack edge intergranular eutectic islands γ/γ' (Fig. 12b) and carbides (Fig. 12c) are presented. In the vicinity of the main crack, a few fine hot cracks are formed. During cooling after welding process, the weld metal solidify under the influence of tensile stresses. These stresses result from the weld shrinkage and irregular cooling of heated material. Under the influence of these stresses, the weld metal deforms and, with insufficient deformation, microfissuring is initiated. The sample was not rigid during the welding and the stresses were result of the temperature gradient. Factors which influence susceptibility to solidification cracking of nickel based superalloys in addition to stresses are chemical composition, solidus-liquidus

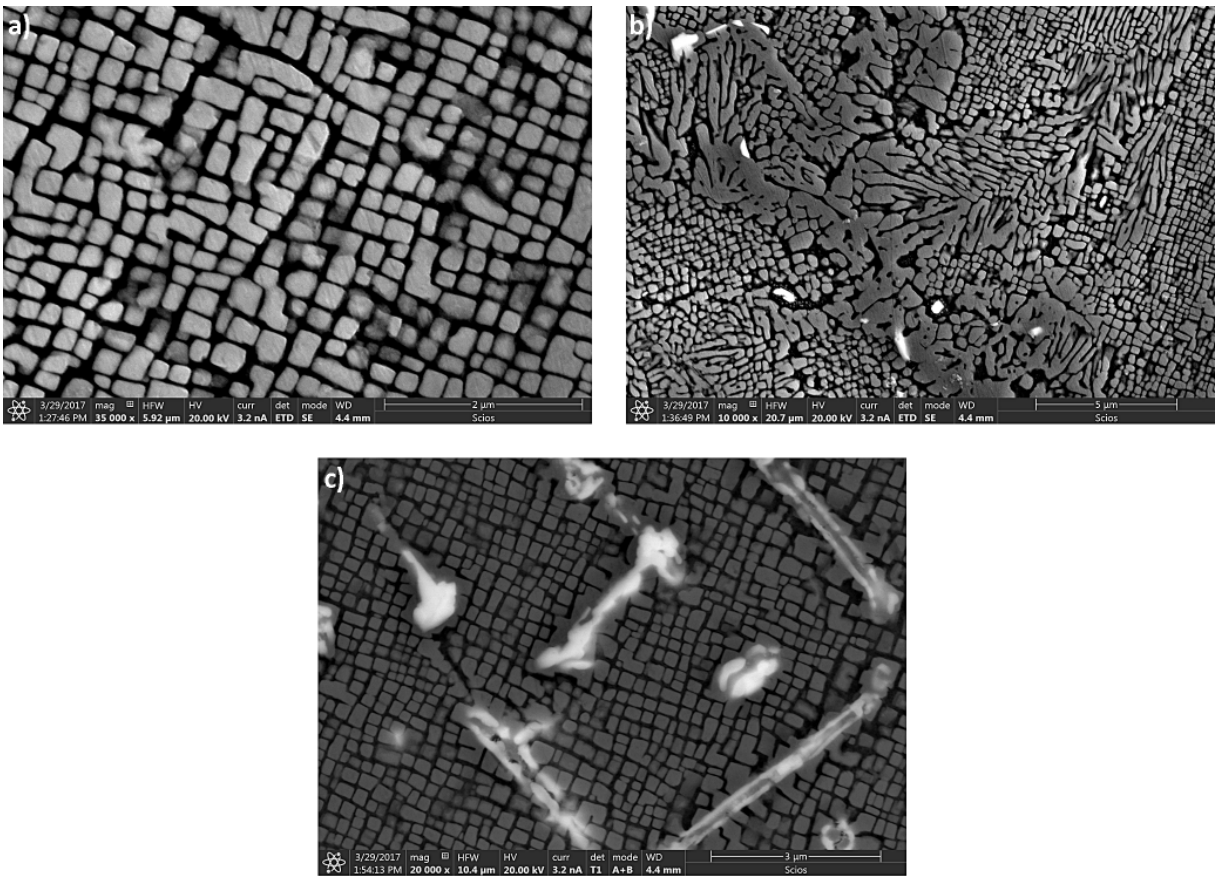

Fig. 8. Microstructure in heat affected zone at 600 μm from fusion line: a) γ' precipitates; b) eutectic island γ/γ'; c) carbides. SEM

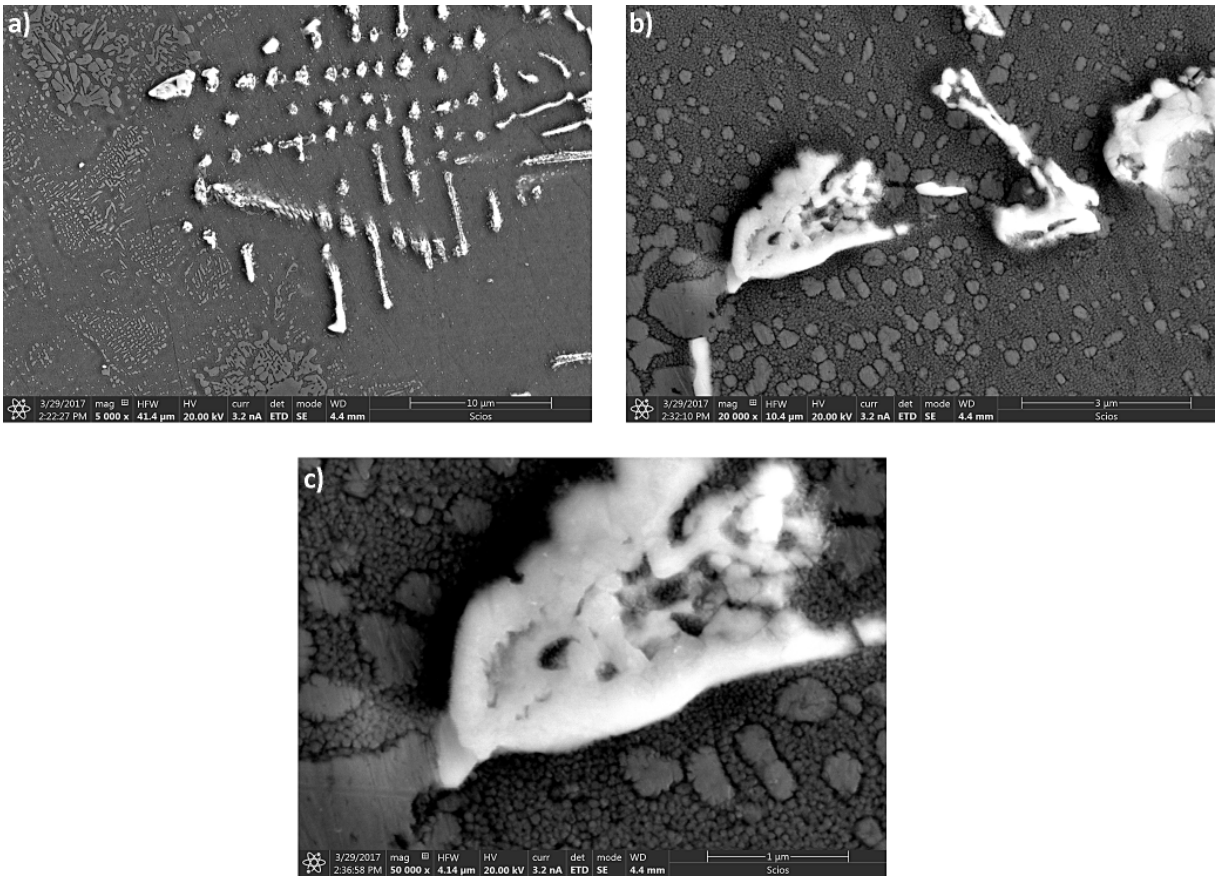

Fig. 9. Microstructural changes in heat affected zone near fusion line: a) Chinese script carbide; b) dissolved γ' particles; c) fine γ' precipitates. SEM

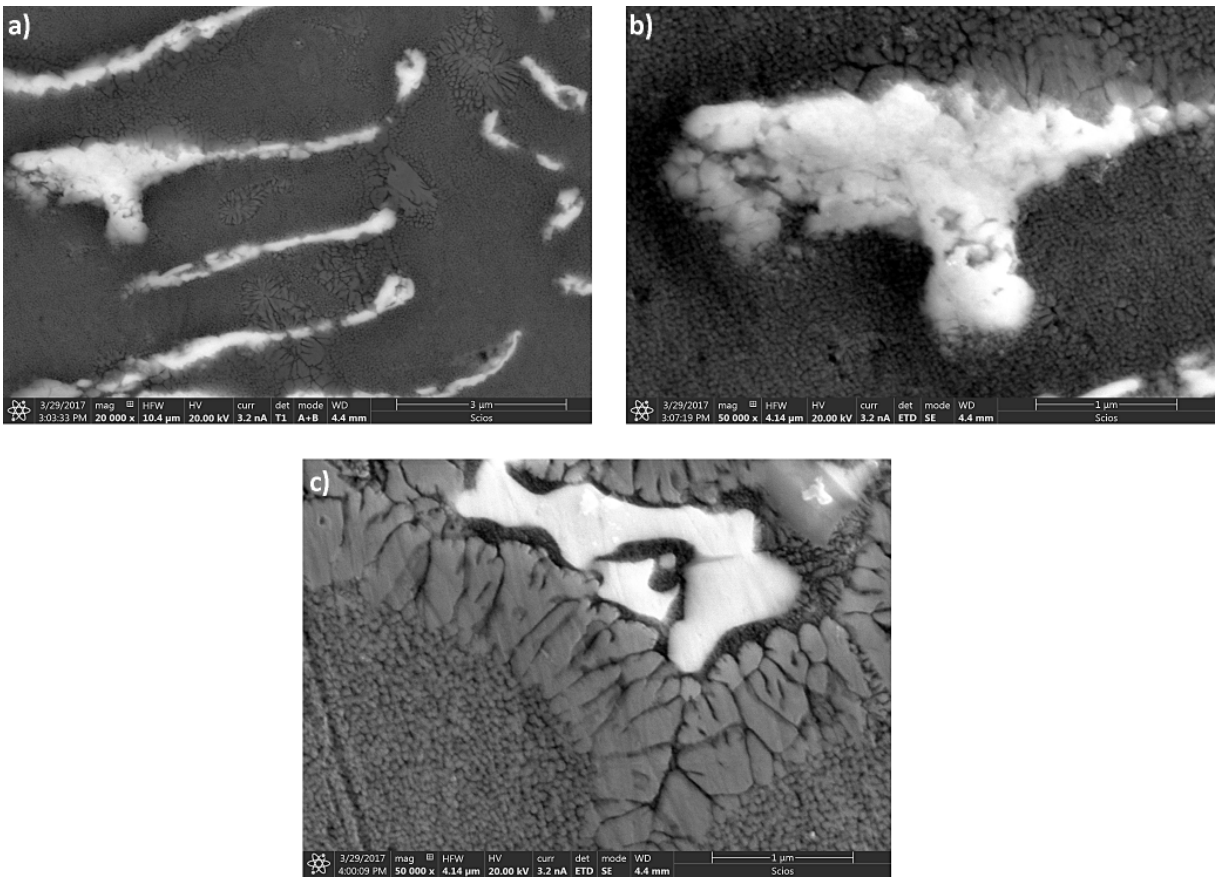

Fig. 10. Microstructure of fusion zone: a) arms of Chinese script carbide; b) fine γ' precipitates adjacent to the carbide; c) regular shape carbide inside eutectic γ/γ'. SEM

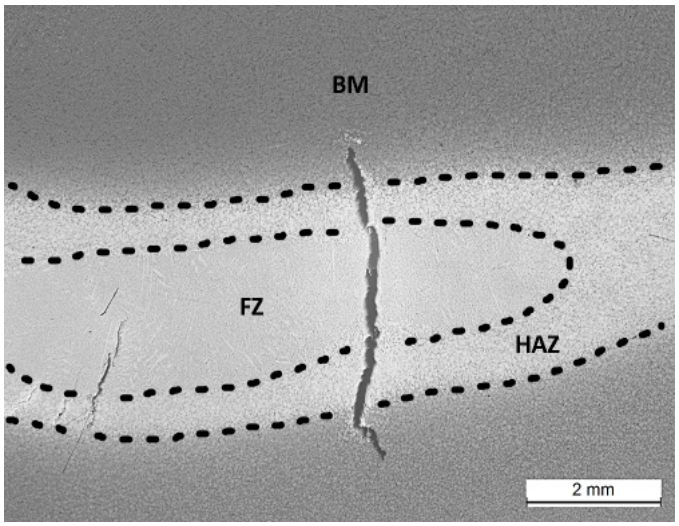

Fig. 11. Localization of cracks LM

temperature range and inhomogeneity of microstructure. MAR-M247 includes high content of γ'-formers aluminum and titanium which influence on strengthening effect during cooling after welding. The solidification cracking response of superalloys is also strongly affected by the temperature range between solidus and liquidus. The impurity elements such as P and S have the greatest impact on extending this range and so in aviation components like turbine vanes their content is strictly controlled. Solidification temperature range (STR) is also extended due to inhomogeneity, namely presence of eutectics. The role of carbides on weldability is well established and this phase has a strong effect on strengthening of grain boundaries. Reduced carbon content to improve weldability have not been proposed because properties, like creep resistance, would be decreased if the concentration of carbon was to be reduced [20-23].

The high welding stresses caused the formation of a hot crack in the fusion zone to affect the initiation of liquation crack in the HAZ near fusion line. More detail SEM investigation revealed several small cracks in the HAZ, where initiation was not affected by the solidification crack but via constitutional liquation phenomena (Fig. 13a-b). Due to the fact that the presence of liquids along grain boundaries is the main feature leading to cracking in HAZ, it is important to take into account the various factors that cause to its formation during welding. Liquid creates as a result of non-equilibrium melting below the solidus temperature of the base material. This phenomenon in the HAZ is considered to be detrimental for weldability because extends the STR and also affects on supersolidus melting by creation a non equilibrium layer that could modify reaction kinetics during multipass welding [24-26]. Liquation below bulk material solidus temperature can be create by two mechanism, namely the grain boundary penetration and segregation mechanism. The first is connected with a phenomenon known as constitutional

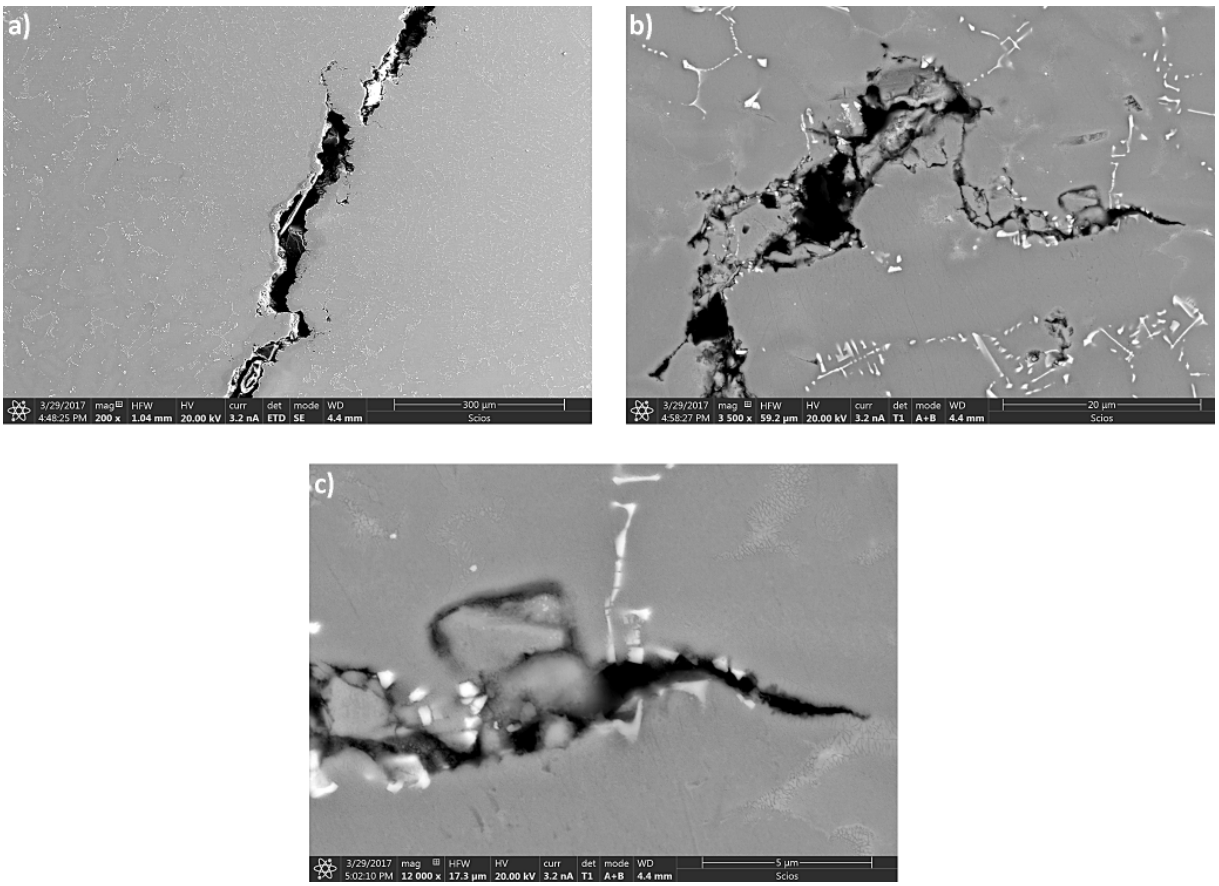

Fig. 12. Solidification crack in fusion zone: a) general view; b) distribution of carbides near crack edge; c) eutectics γ/γ' on tip of crack SEM

liquation of second phase precipitates and penetration grain boundaries by liquid. During heating particles start dissolve at elevated temperatures and then eutectic reaction at the interface matrix-particle is started. The second mechanism is explained by segregation of melting point depressants to grain boundaries which lead to creation of area with lower melting point. These two mechanism are usually separately but in during welding occur in the same time [27-28]. The most common mechanism for solidification of intergranular liquid in the heat-affected zone results in significant microsegregation of the solute ahead of the solid-liquid interface, which is associated with the formation of eutectic microconstituents (Fig. 13c). Solidification of the liquid film via this mechanism can lead to the expansion of the liquidus-solidus temperature range, and thus to the expansion of the brittleness temperature range and increasing of the welding stresses. Rapid re-solidification of metastable HAZ grain boundary liquid can also occur by the liquid film migration (LFM) process. The effect of rapid re-solidification by LFM precluded HAZ liquation cracking by the formation of thick intergranular liquid film which was confirmed by Ojo [29] during investigation conducted on Inconel 738. Despite intensive observations, similar areas in MAR-M247 were not found. In some regions carbides stopped a cracking that developed trough grain boundaries (Fig. 13d). The morphology of the re-precipitation products at the crack edges indicates that carbides had slight contribution to constitutional liquation in MAR-M247. This is most likely due to their high thermal stability. Welding stresses and relatively high hardness of carbides compared to the surrounding material led to brittle secondary cracks on the their surface (Fig. 13e).

4. Summary

In this work, a comprehensive understanding of the heat source effects on Mar-M 247 alloy microstructure and cracking formation is reported. The microstructure of base metal has influence on HAZ microstructure that develops during welding. Alloy in fully heat treatment (FHT) condition consists of significant amount of γ' particles (approximately 60%). Such a volume fraction ensures substantially high mechanical properties in room and service temperatures. MAR-M247 despite FHT state is still characterized by relatively high microstructural inhomogenity originating from segregation of chemical elements during casting of turbine vane. Surface modification via GTAW process induced significant changes of microstructure and hot cracks both solidification in FZ and liquation in HAZ. Hot solidification cracks are not as big weldability problem as liquation cracks in the heat affected zone, because can be eliminated by appropriate selection of filler metal, while base material cannot be altered freely. Liquation cracks are a bigger challenge because the contributing factors are the complex chemical composition

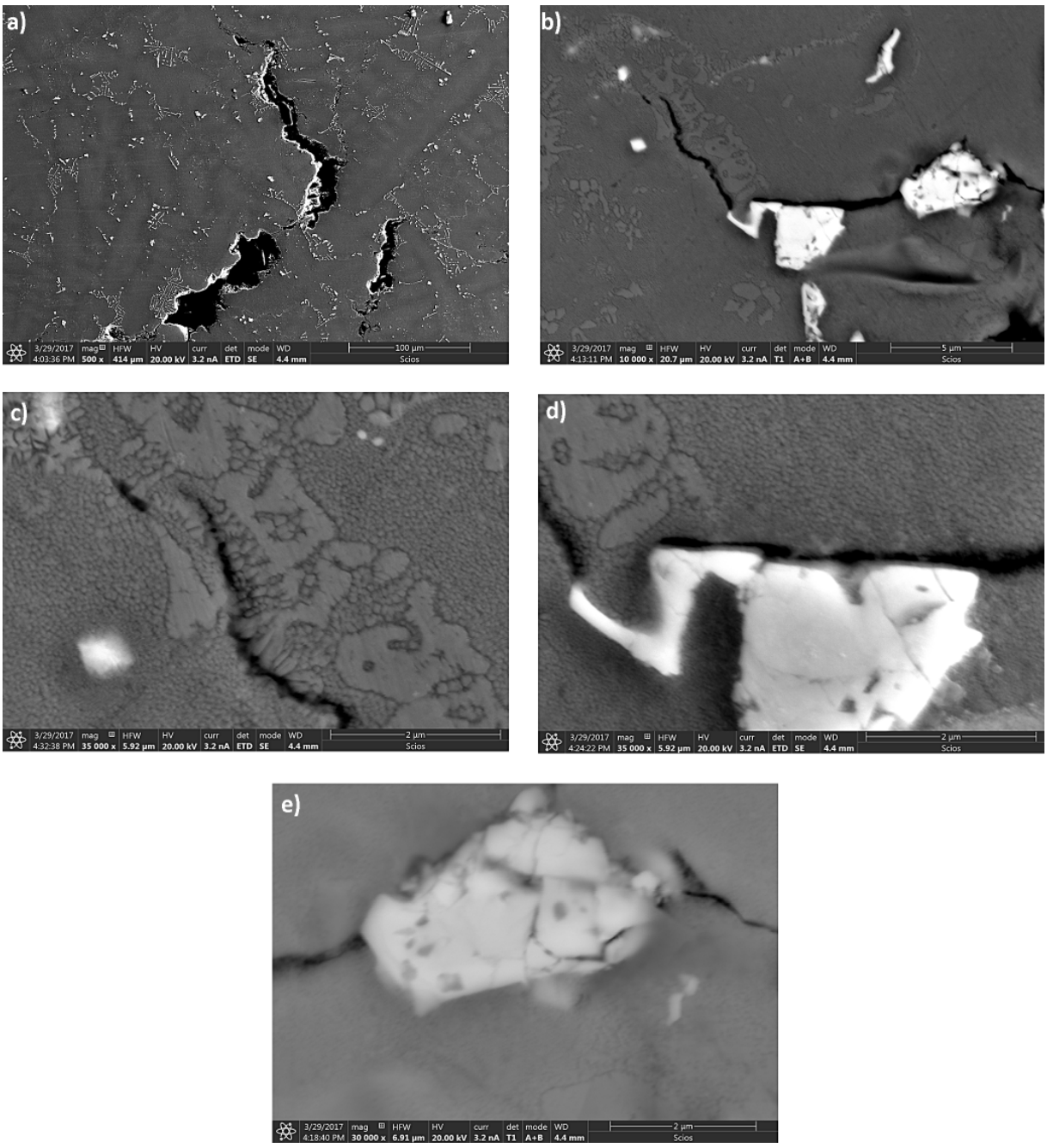

Fig. 13. Liquation cracking in heat affected zone: a) general view; b) tip of crack; c) re-solidification products on crack edge; d) crack stopped by carbide; e) brittle cracking of carbide SEM

and microstructure chosen to achieve high mechanical properties and heat resistance in service conditions. The presence of liquids along grain boundaries is a major cause of liquation cracking in HAZ. Basic requirement for local melting is reaction between a matrix and second phase particle (in this case γ' and MC-type carbides). It is therefore important to take into account the factors that lead to its formation during welding processes. Intermetallic phase γ' and carbides themselves do not melt due to relatively high melting temperature. At the second phase particle-matrix interface under the rapid heating (like welding process) precipitates are not fully dissolved. The particles react with γ-matrix and create conditions to eutectic reaction. The temperature range solidus-liquidus is extended due formation of non-equilibrium liquid layer. Liquation phenomena in HAZ is considered to be detrimental to crack resistance. Cracks are formed as a result of non-equilibrium melting below the solidus temperature of the base material. Re-precipitation of γ'-particles during solidification of metastable liquid and change of thermal expansion enhance stresses that are the key to initiation and cracking propagation.

Acknowledgements

This research work was supported by the Polish Ministry of Science and Higher Education, Grant No. 11.11.110.299.

Conflicts of Interest

The authors declare no conflict of interest.

REFERENCES

[1] R. Reed, The Superalloys: Fundamentals and applications, 2006 Cambridge University Press, Cambridge.

[2] J. Davis, ASM Specialty Handbook: Heat-resistant Materials, 1997 ASM International.

[3] M. Donachie, Superalloys: A technical Guide, 2002 ASM International.

[4] J. Dupont, J. Lippold, S. Kiser, Welding metallurgy and weldability of nickel-base alloys,2009 John Wiley&Sons, New Jersey.

[5] J. Tiley, G.B. Viswanathan, J.Y. Hwang, A. Shiveley, R. Banerjee, Materials Science and Engineering A **528**, 32-36 (2010).

[6] X.P. Tan, J.L. Liu, X.P. Song, T. Jin, X.F. Sun, Z.Q. Hu, J. Mater. Sci. Technol. **27** (10), 899-905 (2011).

[7] A. Royer, P. Bastie and M. Veron, Scripta Materialia **40** (8), 955-961 (1999).

[8] A.T. Egbewande, R.A. Buckson, O.A. Ojo, Materials Characterization **61**, 569-574 (2010).

[9] M. Zhong, H. Sun, W. Liu, X. Zhu, J. He, Scripta Mater. **53**, 159-164 (2005).

[10] O.A. Ojo, N.L. Richards, M.C. Chaturvedi, Scripta Mater. **50**, 641-646 (2004).

[11] O.A. Ojo, R.G. Ding, M.C. Chaturvedi, Scripta Mat. **54**, 2131-2136 (2006).

[12] J.A. Brooks, Weld. J. **53** (11), 517-523 (1974).

[13] J. Pepe, W. Savage, Weld. J. **49** (12), 545-553 (1970).

[14] J. Pepe, W. Savage, Weld. J. **46** (9), 411-422 (1967).

[15] E. Tasak, Metalurgia Spawania, 2008 Wydawnictwo JAK, Kraków.

[16] J.S. Van Sluytman, A. Suzuki, A. Bolcavage, R.C. Helmink, D.L. Ballard, T.M. Pollock, TMS 2008 Superalloys, 499-508 (2008).

[17] R. Baldan, R. Lisboa, R. Tomasiello, J. Mat. Eng. and Perform. **22** (9), 2574-2579 (2013).

[18] A. Royer, A. Jacques, P. Bastie, M. Veron, Mat. Sc. and Eng. 319-321, 800-804 (2001).

[19] A. Royer, A. Jacques, P. Bastie, M. Veron, Sc. Mat. **37** (8), 1199-1205 (1997).

[20] Y. Danis, C. Arvieu, E. Lacoste, T. Larrouy, J.-M. Quenisset, Mat. and Des. **31**, 402-416 (2010).

[21] M. Montazeri, F.M. Ghaini, Mat. Char. **67**, 65-73 (2012).

[22] L.O. Osoba, R.K. Sidhu , O.A. Ojo, Mat. Sc. and Techn. **27** (5), 897-902 (2011).

[23] O.A. Ojo, N.L. Richards, M.C. Chaturvedi, Sc. Mat. **51**, 683-688 (2004).

[24] O.A. Ojo, M.C. Chaturvedi, Metal. and Mat. Trans. A. **38A**, 356-369 (2007).

[25] O.A. Ojo, R.G. Ding, M.C. Chaturvedi, Inter. **16**, 188-197 (2008).

[26] R.K. Sidhu, O.A. Ojo, M.C. Chaturvedi, Metal. and Mat. Trans. A. **40A**, 150-162 (2009).

[27] M. Lachowicz, W. Dudzinski, K. Haimann, M. Podrez-Radziszewska, Mat. Sc. and Eng. **479**, 269-276 (2008).

[28] H. Wang, C. Huang, K. Ho, S. Deng, Mat. Trans. **52** (12), 2197-2204 (2011).

[29] O.A. Ojo, N.L. Richards, M.C. Chaturvedi, Sc. Mat. **51**, 141-146 (2004).